ADVANCED FUNCTIONAL MATERIALS
www.afm-journal.de

Resistance Drift Convergence and Inversion in Amorphous Phase Change Materials

*Julian Pries, Christian Stenz, Lisa Schäfer, Alexander Gutsche, Shuai Wei, Pierre Lucas, and Matthias Wuttig**

Phase change materials (PCMs) are key to the development of artificial intelligence technologies such as high-density memories and neuromorphic computing, thanks to their ability for multi-level data storage through step-wise resistive encoding. Individual resistance levels are realized by adjusting the crystalline and amorphous volume fraction of the memory cell. However, the amorphous phase exhibits a drift in resistance over time that has so far hindered the commercial implementation of multi-level storage schemes. In this study, the underlying physical process of resistance drift with the goal of modeling is elucidated that will help minimize and potentially overcome drift in PCM memory devices. Clear evidence is provided that the resistance drift is dominated by glass dynamics. Resistivity convergence and drift inversion for the amorphous chalcogenide $Ge_{15}Te_{85}$ and the PCM $Ge_3Sb_6Te_5$ are experimentally demonstrated and these changes are successfully predicted with a glass dynamics model. This new insight into the resistance drift process provides tools for the development of advanced PCM devices.

1. Introduction

Phase change materials (PCMs) such as Ge-Sb-Te compounds show a large property contrast between the amorphous and the crystalline phase in, e.g., electrical resistivity and optical reflectivity.[1–5] This difference is explained by a difference in chemical bonding between the covalent amorphous phase and the metavalent crystalline state.[6–14] The ability of PCMs to switch rapidly between the two phases[4,15–17] together with the property difference is exploited in memory storage applications.[15,16] Since the difference between the resistivity of the amorphous and crystalline phase is several orders of magnitude, non-binary multi-level states can be programmed into a single memory device[18] enabling novel computing techniques such as in-memory computing,[19] neuromorphic computing, and artificial intelligence.[20,21] However, the resistance of the amorphous phase is known to continuously increase over time, a process called resistance drift.[22] Resistance drift can lead to a situation where an originally stored state can no longer be clearly read out after a certain time interval has passed.[18] The process of resistance drift therefore poses a challenge to the implementation and commercialization of multi-level data storage. Here, we elucidate the origin of resistance drift and demonstrate how to possibly limit or even reverse it in amorphous chalcogenides including PCMs without the need for demanding device engineering strategies such as heterostructures[23] or projected cells.[24]

The time dependence of the resistance drift in PCMs has been broadly described using a power law (PL) or extended power law (EPL) that indicates a continuous increase in resistivity over time.[25–29] The PL describes the constantly increasing resistance after an onset behavior that is taken into account by the EPL. The drift is attributed to a time-dependent change in the physical properties of the glassy phase.[30–33] Physical changes of glassy phases have been extensively studied in the context of structural relaxation.[34,35] The glassy phase is created when the undercooled liquid (UCL) vitrifies upon cooling. During cooling the atomic mobility decreases until atoms cannot rearrange fast enough to maintain the meta-stable equilibrium so that the structure of the UCL becomes "frozen-in" at the so-called fictive temperature T_f.[36] The newly formed glassy state is thermodynamically unstable, i.e., it is kinetically prevented from evolving toward its equilibrium state on laboratory time scales provided that it is kept sufficiently far below the glass transition temperature T_g.[36,37] However, when a glass is subjected to an annealing temperature T_a close to T_g, the fictive temperature can evolve toward T_a in relatively short time[36,38,39] as the glass structure of the glassy

J. Pries, C. Stenz, L. Schäfer, M. Wuttig
Institute of Physics IA
RWTH Aachen University
52074 Aachen, Germany
E-mail: wuttig@physik.rwth-aachen.de
A. Gutsche, M. Wuttig
PGI-10
Forschungszentrum Jülich
52425 Jülich, Germany
S. Wei
Department of Chemistry
Aarhus University
DK-8000 Aarhus-C, Denmark
P. Lucas
Department of Materials Science and Engineering
University of Arizona
Tucson, AZ 85721, USA
The ORCID identification number(s) for the author(s) of this article can be found under https://doi.org/10.1002/adfm.202207194.

DOI: 10.1002/adfm.202207194

state relaxes toward that of the UCL. When $T_a < T_f$, this process is called aging. During aging, enthalpy H is released and the (specific) volume decreases.[40,41] When aged long enough, the glassy phase reaches the state of the UCL and T_f becomes equal to T_a upon stabilization.[36] However, when T_a is low, the structural relaxation time τ is very large and can easily exceed the experimental time scale. In this case, the stabilization of the glassy phase may not be observed experimentally. Conversely, if the annealing temperature T_a is increased to above the fictive temperature T_f, the direction of structural relaxation is inverted causing the material to absorb enthalpy H and increase in volume.[40,41] Since this process is opposite to aging it is called rejuvenation.

In this study, we use $Ge_{15}Te_{85}$ as a PCM-analog with good glass-forming ability to establish a direct correlation between structural enthalpy relaxation and changes in resistivity. $Ge_{15}Te_{85}$ enables unambiguous measurements of T_f to perform modeling of the glassy dynamics and demonstrate a parallel with resistance drift. We show that enthalpy and resistivity concurrently exhibit not only aging but also stabilization following a pattern predicted by a conventional glass relaxation model. We further show that rejuvenation causes resistance drift inversion in both $Ge_{15}Te_{85}$ and the PCM $Ge_3Sb_6Te_5$. Finally, the resistivity drift of $Ge_3Sb_6Te_5$ is fitted with a model accounting for dynamic heterogeneities that is an inherent feature of glassy relaxation, thereby substantiating the role of structural relaxation as the origin of resistance drift.

2. Results

2.1. Convergence and Inversion of Enthalpy and Resistivity in $Ge_{15}Te_{85}$: Modeling and Experiment

For measuring the enthalpy changes induced by structural relaxation, amorphous $Ge_{15}Te_{85}$ was prepared by magnetron sputter deposition as previously described in Refs. [42,43]. Differential scanning calorimetry (DSC) was used to obtain the excess specific heat capacity $C_p^{exc}(T)$, by subtracting the crystalline rescan from the initial measurement, both collected at a heating rate ϑ of 40 °C min^{-1}, see **Figure 1**a. During the upscan, the as-deposited (un-annealed) phase shows a constant $C_p^{exc}(T)$ up to 75 °C where an exothermic event of enthalpy relaxation occurs. This enthalpy release is the well-known consequence of reheating a glass at a lower rate than its (effective) cooling rate.[42,44] Upon entering the glass transition region, the expected endothermic jump is observed. Note that there is no sign of crystallization in the temperature range up to 170 °C shown here. This enables unambiguous determination of the fictive temperature T_f. Isothermal pre-annealing at 105 °C for 2–4320 min largely alters the thermal response of the glassy phase as is seen from the disappearing exothermic enthalpy relaxation and the developing sharp endothermic overshoot upon entering the UCL. These overshoots correspond to a recovery of the enthalpy lost during annealing through structural relaxation.

To quantify the loss in enthalpy H induced by pre-annealing, the excess specific heat capacity curves are integrated and normalized to a point in the UCL where all samples have reached the same equilibrium enthalpy level. Furthermore, the glassy state of the as-deposited material is chosen as the reference state and its excess enthalpy is set to 0. The resulting enthalpy curves $H^{exc}(T)$ during the upscan after pre-annealing are presented in Figure 1b. In this plot, the enthalpy ΔH_{rel} released during pre-annealing can be read off directly from the ordinate. During the isothermal hold at 105 °C, enthalpy is released which shows that the glassy phase is *aging*. Furthermore, when pre-annealed for 4320 min (=3 days), so much enthalpy of the glassy phase is released that the enthalpy level becomes equal to that of the extrapolated UCL at T_a, which demonstrates that the material has "stabilized" and reached thermal equilibrium. Thus, the fictive temperature has converged to the annealing

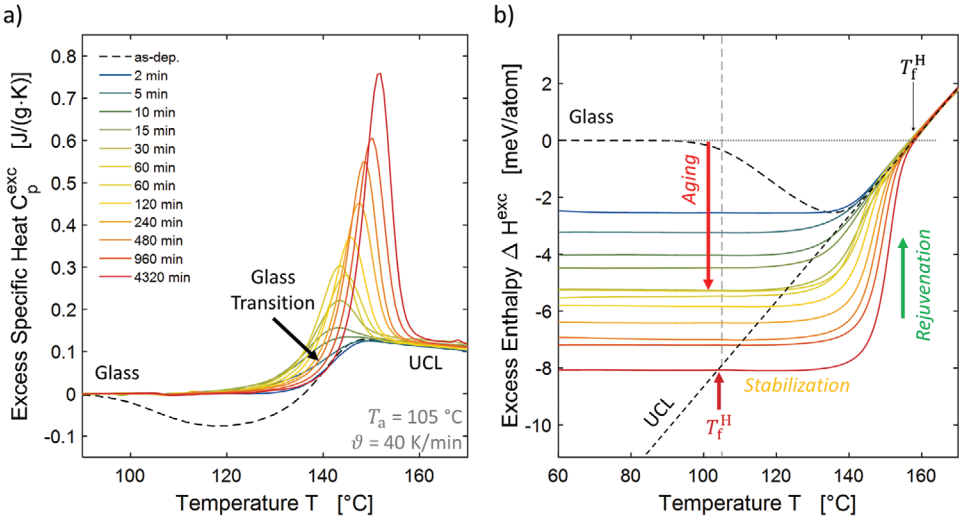

Figure 1. a) Excess specific heat capacity $C_p^{exc}(T)$ (endothermic is up) and b) excess enthalpy $H^{exc}(T)$ of as-deposited $Ge_{15}Te_{85}$ pre-annealed at 105 °C for increasing periods of time. The heating rate ϑ is 40°C min^{-1}. The material releases enthalpy upon structural relaxation of the glassy phase during pre-annealing. For longest annealing times, the enthalpy level of the glass and the UCL equalize showing that the glass stabilizes. Reheating a glass that has been previously stabilized leads to rejuvenation through enthalpy regain, as revealed by the large endothermic peaks in a). For modeling purpose, the fictive temperature T_f^H is calculated from the point of intersection of the extrapolated temperature dependence of $H^{exc}(T)$ for the glass and the UCL, as indicated in (b).

temperature T_a. When this aged and stabilized glassy phase is heated at a constant heating rate of 40 °C min^{-1}, a steep increase in enthalpy (absorption of enthalpy) is observed starting at ≈135 °C. The observation of enthalpy absorption shows that the glassy phase rejuvenates. This illustrates the three stages of structural evolution during heat treatment of glassy $Ge_{15}Te_{85}$.

In order to provide a theoretical framework to these empirical observations, a conventional model of glassy dynamics[36] is applied to the relaxation of structural enthalpy, namely the Tool–Narayanaswamy–Moynihan (TNM)[37,45–47] model. The TNM model in its Adam–Gibbs (TNM-AG) based form[41,48,49] consists in iteratively predicting the evolution of a glassy structure subjected to an arbitrary temperature profile.[38,39] For that purpose the structural state of the glass is quantitatively specified in temperature units using the concept of fictive temperature T_f.[45,50] The TNM-AG model and the concept of the fictive temperature are presented in detail in the Supporting Information. The fictive temperature derived from enthalpy T_f^H is found from linearly extrapolating the temperature dependence of the enthalpy of a glassy phase at low temperature and of the UCL at high temperatures,[42] as indicated in Figure 1b. The temperature where both extrapolations intersect is taken as the fictive temperature T_f^H of that glassy state. The values obtained are presented in **Figure 2**a as a function of isothermal pre-annealing time at T_a = 105 °C. The fictive temperature decreases from T_f^H = 159 °C for the as-deposited phase, indicating aging, and becomes equal to the annealing temperature at long annealing times, indicating stabilization. The same analysis as that described in Figure 1 was also performed at an annealing temperature of 85 °C ($C_p^{exc}(T)$ and $H^{exc}(T)$ curves are shown in Figure S2, Supporting Information). The resulting fictive temperature change over time is plotted in Figure 2b. At that temperature it is clear that the glass has not yet equilibrated at the end of the heat treatment. The fictive temperature T_f^H is still far higher than the annealing temperature T_a = 85 °C even after an annealing time of 4320 min. Here, the TNM-AG model indeed confirms that the glass is still in the process of relaxing (aging) and has not yet stabilized. Now that the enthalpy relaxation of glassy phase $Ge_{15}Te_{85}$ is understood both qualitatively and quantitatively, the resistance relaxation of $Ge_{15}Te_{85}$ is investigated next.

With the intention of contrasting the enthalpy behavior with the resistance drift, electrical measurements were performed on thin films of $Ge_{15}Te_{85}$. The resistivity, which is proportional to the resistance, is measured with a custom-made van-der-Pauw (vdP) setup[51] equipped with a heating unit to enable temperature and time control. The resistivity of as-deposited $Ge_{15}Te_{85}$ during an isothermal hold at 85°C is shown in **Figure 3**a. Here, the commonly reported case of a PL dependence of resistivity with time is observed and the onset behavior at low annealing times is described by the EPL mentioned above, see Refs. [25–29]. This behavior is consistent with the common view that upon aging of the glassy phase the resistance drifts seemingly continuously over time[25–29] and indeed in the enthalpy relaxation measurements at 85 °C, only aging was observed. In contrast, the temporal change of the resistivity during an isothermal hold at 105 °C presented in Figure 3b shows a different behavior. The usual onset behavior is followed by a region of constant slope obeying a PL as in the case of the 85 °C isotherm, but at annealing times larger than 3000 s, the slope of the resistivity starts decreasing to zero, clearly indicating that the drifting resistivity is converging to a constant value. The convergence of the resistivity qualitatively coincides with the convergence of the enthalpy H and the fictive temperature T_f^H upon glass stabilization shown in Figure 1b and Figure 2a, respectively. This shows that the resistance converges upon glass stabilization.

In order to quantitatively link the convergence in resistance to the structural stabilization of the glassy phase, we apply the TNM-AG glass dynamic model to fit the change in resistivity. This requires extracting an equivalent resistivity fictive temperature T_f^ρ from resistivity measurements to provide adequate

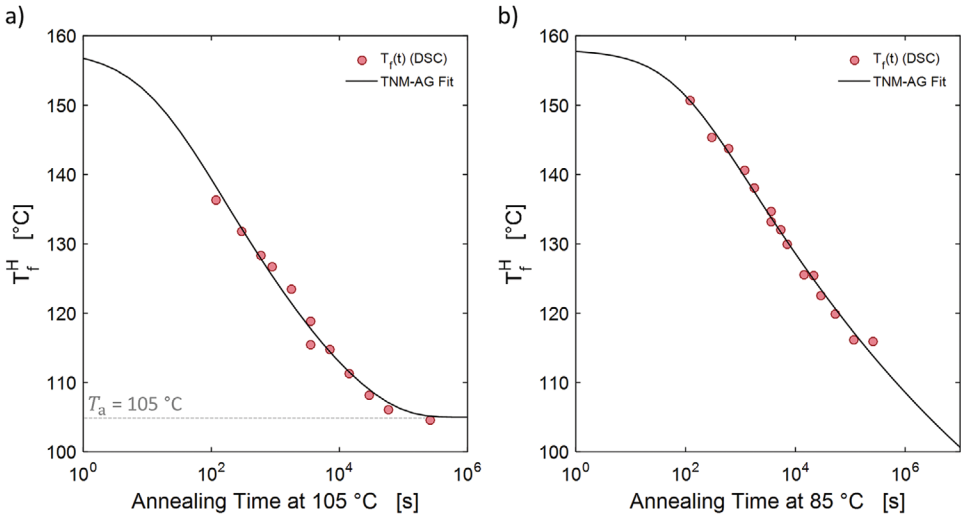

Figure 2. Evolution of the fictive temperature of enthalpy T_f^H of $Ge_{15}Te_{85}$ glass as a function of pre-annealing time at a pre-annealing temperature of 105 °C (a) and 85 °C (b). The TNM-AG model is fitted to the relaxing fictive temperature data. At 105 °C, the fictive temperature decreases continuously and converges to the annealing temperature upon glass aging and stabilization. At 85 °C, the fictive temperature does not converge due to the long relaxation time compared to observation time. At that temperature, $Ge_{15}Te_{85}$ has not reached thermal equilibration.

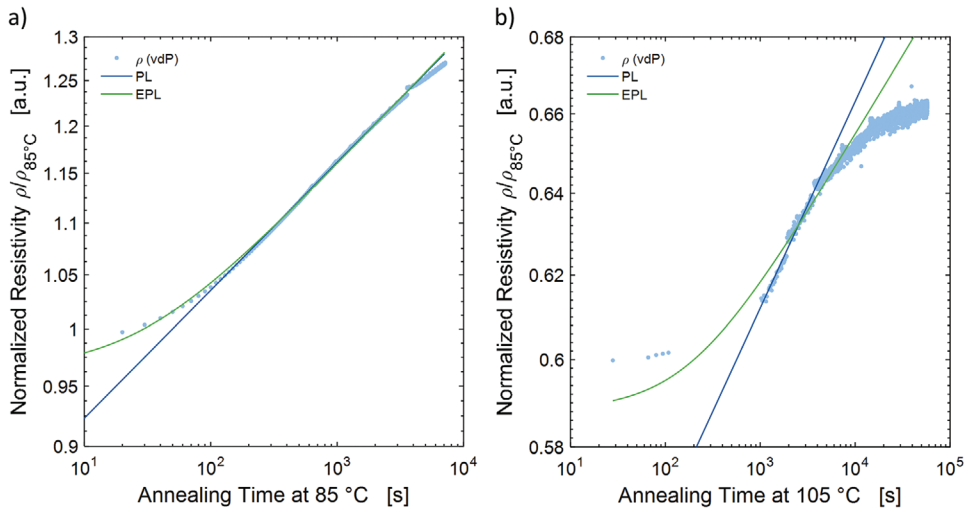

Figure 3. Resistivity drift of $Ge_{15}Te_{85}$ glass during isothermal annealing at a temperature of a) 85 °C and b) 105 °C. At 85 °C (≈45 °C below T_g), after an onset behavior the resistivity increases continuously following the commonly observed power law (PL) behavior. Conversely, when annealed at 105 °C (≈25 °C below T_g), the resistivity convergences to a maximum value upon glass stabilization.

data points for the TNM-AG model. This process described in detail in Supporting Information consists in measuring the resistivity change during heating ramps after annealing treatments for increasing time periods. The temperature of intersection between the extrapolated glassy and liquid phases yields the T_f^ρ value (see Figure S3, Supporting Information). This approach is analogous in principle to that applied to calorimetric data in Figure 1b.

The fictive temperature values T_f^ρ obtained are plotted in **Figure 4**a and are fitted with the TNM-AG model. Analogously to enthalpy relaxation, the fictive temperature of resistivity T_f^ρ decreases with annealing time, indicating aging, and converges to the annealing temperature of T_a = 105 °C, indicating stabilization. This behavior is well described by the TNM-AG model. Also, to compare the T_f^ρ data and TNM-AG curve with measured resistivity data $\rho(t)$ of Figure 3b, the resistivity is calculated from T_f^ρ. The calculation scheme is presented in the SI. These resulting data points (red circles) and curve (black line) line up well with the isothermally obtained values (light blue dots) as shown in Figure 4b. The TNM-AG curve lines up with the experimental data for times longer than 1000 s. The mismatch in the shorter timescale is an experimental artefact due to structural or resistivity relaxation occurring already during the upscan at 5 °C min^{-1} when heating the sample up to 105 °C. Overall, these results show that the resistivity drift and convergence is quantitatively and qualitatively explained

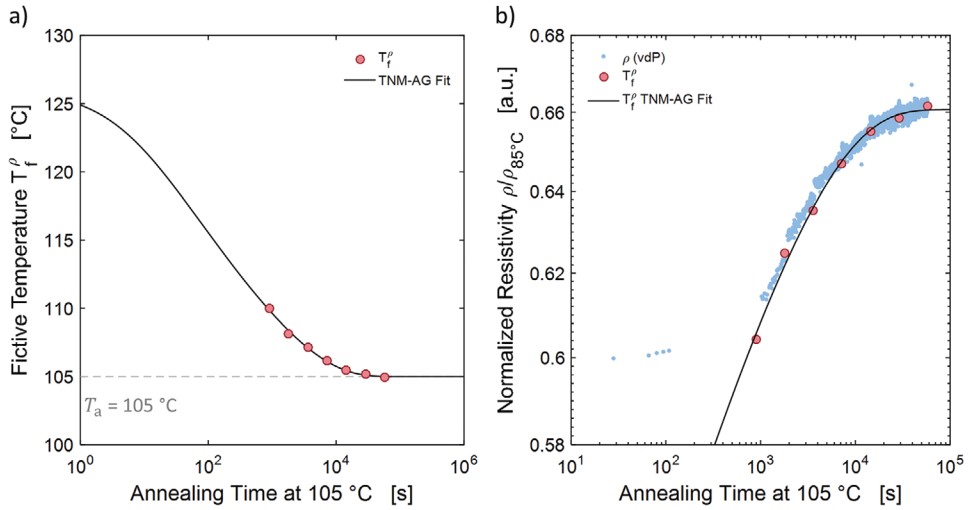

Figure 4. a) Evolution of the fictive temperature T_f^ρ derived from resistivity upscan measurements performed after annealing $Ge_{15}Te_{85}$ glass at 105 °C for increasing time periods. The T_f^ρ data are accurately fitted with the TNM-AG model (black line) and converge toward the annealing temperature 105 °C for long times, thereby confirming stabilization. b) Comparison of the resistivity data obtained during the isothermal hold at 105 °C (light blue dots) with resistivity values calculated from T_f^ρ (red circles) and the TNM-AG model (black line) derived in a). The experimental resistivity data show an excellent match with the prediction from the glass relaxation model. Note that the initial T_f^ρ is lower than T_f^H shown in Figure 2. This is due to the introduction of heat to the chalcogenide during deposition of a capping layer on the vdP samples.

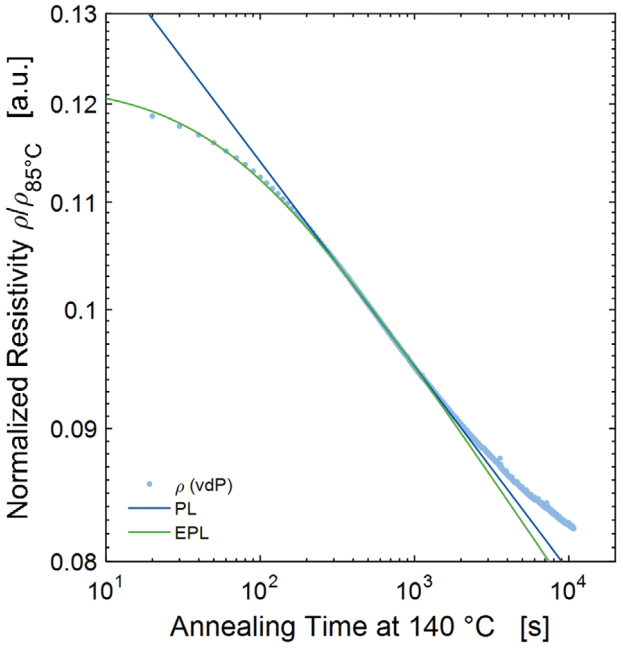

Figure 5. Resistivity drift inversion of as-deposited $Ge_{15}Te_{85}$ observed during an isothermal hold at 140 °C (≈10 °C above T_g). The resistivity is decreasing as opposed to the increase in resistivity found at 85 °C and 105 °C in Figure 3. Here, the annealing temperature is higher than the resistivity fictive temperature T_f^{ρ} and therefore the glass is rejuvenating by structural relaxation instead of aging, which means that the relaxation direction is inverted. This inversion of the relaxation direction is the reason for the inverted resistivity relaxation.

correctly by structural relaxation of the glassy phase and glass dynamics.

So far, upon glassy phase aging the enthalpy is found to decrease and the resistivity to increase in a predictable way. Upon thermal equilibration of the glass structure, enthalpy and resistivity relaxation comes to a halt. It remains to be seen, if the correlation between enthalpy and resistivity still holds during glass rejuvenation. If this is the case, the resistivity drift should be inverted when the glassy structure regains enthalpy. As stated above, the glassy phase rejuvenates when the annealing temperature exceeds the fictive temperature. In order to induce rejuvenation, we raise the isothermal annealing temperature to 140 °C, which is higher than the T_f^{ρ} of 128 °C for the as-deposited phase, and measure the resistivity $\rho(t)$ to monitor a potential drift inversion. The results are shown in **Figure 5**. Indeed, in contrast to the two previous cases presented in Figure 3, the resistivity decreases with annealing time. This clearly demonstrates that the resistivity drift is inverted upon rejuvenation of the glassy phase.

2.2. Convergence and Inversion of Enthalpy and Resistivity in $Ge_3Sb_6Te_5$

The data shown above for $Ge_{15}Te_{85}$ demonstrate the intricate interplay between structural relaxation and resistivity evolution. However, $Ge_{15}Te_{85}$ is not a functional PCM used in memory devices, since it forms a rather stable glassy phase and thus crystallizes slowly. Hence, in the following we focus on a Ge-Sb-Te based PCM, namely $Ge_3Sb_6Te_5$. We selected this material because it has recently shown promise as a PCM due to the very high crystal growth speeds mandatory for memory applications.[52] Furthermore, it features a fragile-to-strong transition (FST),[52] which is beneficial for fast crystallization at high temperatures and amorphous phase stability at low temperatures.[53] The change in excess specific heat capacity $C_p^{exc}(T)$ of the $Ge_3Sb_6Te_5$ glassy phase is shown in **Figure 6**a during upscans at 40 °C min^{-1} similar to $Ge_{15}Te_{85}$ shown in Figure 1 a. The scan of as-deposited (un-annealed) $Ge_3Sb_6Te_5$ shows a significant exothermic enthalpy relaxation initiated near 85 °C similar to $Ge_{15}Te_{85}$. The glass transition then occurs near 190 °C, followed by crystallization at ≈235 °C. The effect of 1 h pre-annealing at different temperatures is shown in Figure 6a. When pre-annealed at 175 °C or higher, the development of a large endotherm is observed, clearly indicating the enthalpy recovery from the previous annealing processes. This effect is analogous to $Ge_{15}Te_{85}$, see Figure 1a. As the plateau in $C_p^{exc}(T)$ of the UCL is obscured by crystallization, the enthalpy fictive temperature T_f^H cannot be determined unambiguously from the extrapolation method applied previously. Nevertheless, it can be inferred that the as-deposited glassy phase of $Ge_3Sb_6Te_5$ is prone to glass aging. We note that an increase in pre-annealing temperature from 170 to 195 °C leads only to a small change in the $C_p^{exc}(T)$ curve, which signals a decreased relaxation amplitude and thus beginning glass stabilization. Therefore, it should be possible to investigate the resistivity relaxation and stabilization during structural relaxation in this range of temperature.

A resistivity measurement during an isothermal annealing at 130 °C, i.e., ≈60 °C below the glass transition temperature, is shown in Figure 6b, which reveals the common case of a continuous increase in resistivity upon aging with its characteristic onset followed by a PL behavior. In $Ge_{15}Te_{85}$, the resistance convergence is observed at 105 °C, which is ≈25 °C below its glass transition temperature. Therefore, the annealing temperature is also raised to ≈25 °C below T_g, i.e., to 165 °C to observe resistivity convergence in $Ge_3Sb_6Te_5$. Indeed, a clear deviation from the constant slope regime at large annealing time is evident, which implies that the resistivity approaches a constant value, see Figure 6c. This behavior is qualitatively consistent with that of as-deposited $Ge_{15}Te_{85}$ at 105 °C, which supports the conclusion that the resistance of this PCM is also converging upon stabilization of the glassy phase.

In an attempt to initiate glass rejuvenation, we raised the temperature of isothermal van-der-Pauw measurements above T_g; however, the material was found to crystallize at 170 °C when annealed for longer than 1 h. Since T_a cannot be raised high enough to induce rejuvenation, the alternative is to decrease T_f. Indeed, according to the results presented above for $Ge_{15}Te_{85}$, the resistance drift inversion should be observed when T_a becomes larger than the fictive temperature of the glassy phase. To decrease the fictive temperature, a sequential annealing scheme was applied: first, the sample was isothermally annealed for 1 h at 50 °C before it was cooled back to room temperature (RT). The annealing temperature was then increased by 10 °C to 60 °C and the sample was annealed for another hour and cooled back to RT and so forth. The resistivity relaxation was monitored during each isothermal annealing

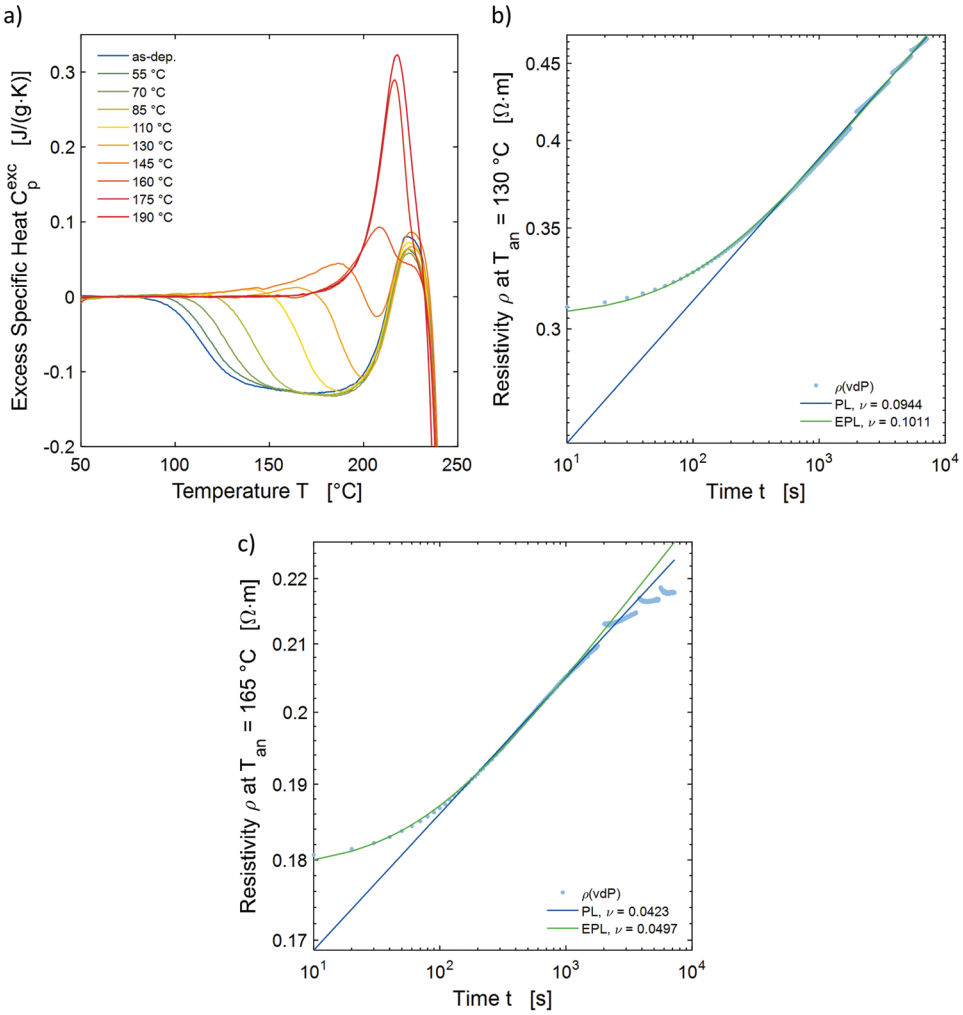

Figure 6. a) Evolution of the excess specific heat capacity $C_p^{exc}(T)$ of $Ge_3Sb_6Te_5$ after pre-annealing for 1 h at increasing temperature. The pre-T_g exotherm progressively disappears as the glass is subjected to aging at higher temperature. The full glass transition is obscured by fast crystallization; b) Resistivity drift of as-deposited $Ge_3Sb_6Te_5$ during isothermal hold at 130 °C. The resistivity shows the onset followed by the common power law (PL) behavior. c) Resistivity drift of as-deposited $Ge_3Sb_6Te_5$ during isothermal hold at 165 °C. After the onset and power law behavior, the resistivity starts converging to a constant value upon glass stabilization at annealing times larger than 2000 s. The small discontinuities are caused by unstable temperature conditions after heating up from intermediate cooling to room temperature (RT).

step (see Supporting Information[52] for the complete data set). Since the relaxation time is large at temperatures far below T_g, the glass is not expected to stabilize within one hour but the fictive temperature should continuously decrease. It is then expected that T_a will at some point become larger than T_f^p and the resistance drift inversion may be observable. The evolution of the resistivity after reaching the annealing temperature of 160 °C is shown in **Figure 7**a. Resistance drift inversion is initially observed up to 600 s but surprisingly reverses and increases to above the initial value. If resistance drift and crystallization were overlapping, the opposite behavior would be expected, i.e., an increasing resistivity upon aging at first followed by a rapid decreasing resistivity upon crystallization. This excludes crystallization as a possible explanation. This behavior is instead reminiscent of the "cross-over" effect, an inherent feature of glass relaxation dynamics first reported more than half a century ago.[54,55] When a glass is relaxed significantly but not to full stabilization, the structural heterogeneity of the glass phase[56–59] results in a distribution of dynamic processes where fast-relaxing domains are already able to stabilize (small relaxation time τ) while slow-relaxing domains are still in the initial stage of structural relaxation (large τ). If afterwards the annealing temperature is increased, the fast-relaxing domains adjust quickly by rejuvenation. This leads to the fast initial resistivity drift inversion up to 600 s. As these domains quickly stabilize, the relaxation behavior becomes dominated by the slow-relaxing domains that are still engaged in aging thereby leading to the observed increase in $\rho(t)$. The cross-over effect was previously modeled by Macedo and Napolitano (MN) using a relaxation function dominated by two relaxation times τ_1 and τ_2,[60] which in the present case can be formulated as:

$$\rho(t) = \rho_\infty + \frac{1}{2}\left(\rho_1 \exp\left(-\frac{t}{\tau_1}\right) + \rho_2 \exp\left(-\frac{t}{\tau_2}\right)\right) \quad (1)$$

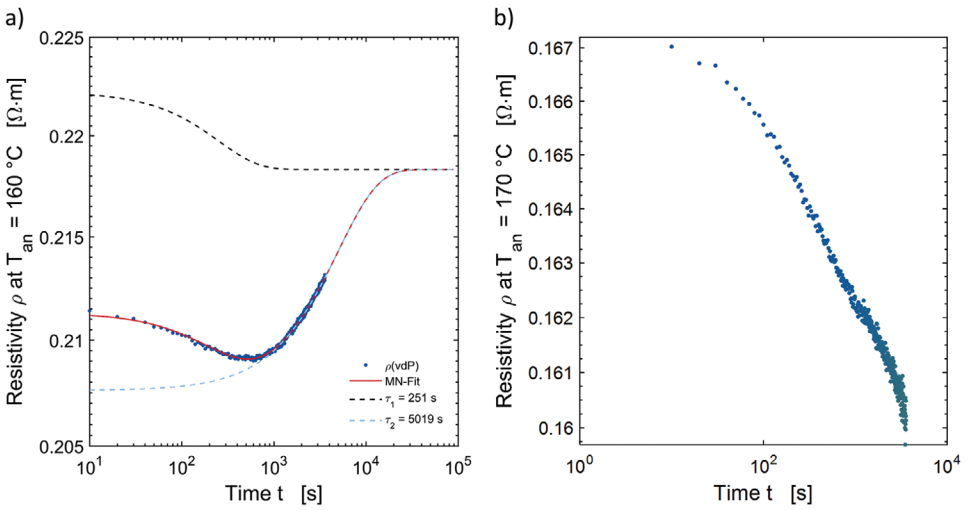

Figure 7. Resistivity drift of $Ge_3Sb_6Te_5$ during isothermal hold at a) 160 °C and b) 170 °C after the sequential annealing protocol described in the main text and the Supporting Information. The sequential annealing steps progressively reduces T_f^{ρ} while the annealing temperature is increased to induce rejuvenation and drift inversion. The first evidence of drift inversion is observed when the temperature is raised to 160 °C. The resistivity decreases at first but at 600 s starts to increase again. This is the so-called cross-over effect, which is caused by the dynamic heterogeneity of the glassy phase. When the temperature is raised to 170 °C afterwards in b), the resistivity only decreases.

where ρ_∞ is the resistivity after glass stabilization and ρ_i are the initial resistivity levels associated with the relaxation times τ_i. The red line in Figure 7a shows that the MN function permits to fit the resistivity almost perfectly. This cross-over effect demonstrates the presence of a distribution of relaxation times in the glassy phase[36,60] and its direct effect on the resistivity relaxation. Dynamic heterogeneities are an intrinsic feature of glass-forming systems;[57] therefore, the cross-over effect observed in $Ge_3Sb_6Te_5$ constitutes additional evidence that the resistance relaxation is governed by glass dynamics and structural relaxation. The same cross-over effect can be observed in $Ge_{15}Te_{85}$ as well (see Supporting Information). The presence of the cross-over effect indicates that the applied annealing temperature of 160 °C is near the average fictive temperature T_f^{ρ}. This suggests that by increasing the annealing temperature by an additional 10 °C, rejuvenation may become the governing structural relaxation mechanism. Indeed, Figure 7b shows a monotonic decrease in resistivity during annealing at 170 °C for 1 h as expected from resistance drift inversion caused by rejuvenation of the glassy phase, similar to the case of $Ge_{15}Te_{85}$ shown in Figure S7 in the Supporting Information. Crystallization is not observed at 170 °C in as-deposited $Ge_3Sb_6Te_5$ below 1 h of annealing. Since for PCMs, sub-T_g annealing is found to reduce the crystallization ability,[61,62] crystallization is therefore unlikely to affect the decrease in resistivity shown in Figure 7b. The observations for $Ge_3Sb_6Te_5$ thus confirm those obtained for $Ge_{15}Te_{85}$, demonstrating that resistance drift is dominated by glass dynamics and structural relaxation and is likely to be a universal feature of amorphous chalcogenides including PCMs.

3. Discussion and Conclusion

Upon structural relaxation, the thermodynamically unstable glassy phases rearrange spontaneously but slowly to approach the structure of the meta-stable UCL. A change in the atomic structure of a disordered (amorphous) semiconducting material is expected to change the conductivity of the material. The decrease in molar volume during aging is expected to increase the bandgap energy[63] and in turn reduce the charge carrier density; but also decrease the electron scattering length and mobility. Both effects are consistent with the observed increase in resistivity during structural relaxation of PCMs. Overall, the present experimental data for amorphous $Ge_{15}Te_{85}$ and the promising PCM $Ge_3Sb_6Te_5$ demonstrate that glassy phase aging, stabilization and rejuvenation cause resistance drift, resistance convergence and drift inversion, respectively. Furthermore, the resistance relaxation exhibits a cross-over behavior that can be understood in terms of dynamic heterogeneity of the glassy phase again highlighting the connection between glass dynamics and resistivity evolution. Also, the relaxation of resistance can be described by the behavior of the fictive temperature using conventional glass relaxation models such as the TNM(-AG) analogously to the enthalpy relaxation. Thus, these results provide strong evidence that temporal changes of the resistance in these amorphous chalcogenides are governed by glass dynamics, presumably by the process of structural relaxation. The fact that it can be described by mathematical approaches, enables the modeling, minimization, and the potential overcoming of resistivity drift in PCM memory applications. Minimizing or eliminating resistance drift by controlling glass dynamics opens up new opportunities for developing more robust PCM-based non-volatile multi-level data storage devices, which are essential for in-memory computing and artificial intelligence applications.

4. Experimental Section

The resistance and resistivity were measured in van-der-Pauw (vdP) geometry[51] as a function of temperature and time in a homemade setup

under Argon atmosphere. The samples consisted of a glass substrate on which the electrical chromium contacts, the chalcogenide layer and the $(ZnS)_{80}$:$(SiO_2)_{20}$ capping layer were deposited via magnetron sputter deposition. The deposited chalcogenide film was of square shape with an edge length of ≈1 cm. For magnetron sputter deposition stoichiometric targets were employed and the base pressure was 3×10^{-3} mbar. The accompanying differential scanning calorimetry (DSC) measurements for investigating the enthalpy relaxation were conducted on a PerkinElmer Diamond DSC. The temperature reading in DSC measurements was corrected by the melting onset of pure Indium at a constant heating ϑ. Contrary to the vdP samples, for DSC samples several micrometer thick layers of the chalcogenides were deposited onto metal sheets and subsequently peeled off. These samples do not feature a capping layer.

Statistical Analysis: Power data taken by DSC is converted to specific heat capacity in Pyris Series Software by PerkinElmer and is further analyzed in a self-developed program in Matlab by Mathworks. In this Matlab program, the integration of the heat capacity data was performed and the changes in the enthalpy and the fictive temperature values were measured.

Fitting the PL and the EPL, as well as any Arrhenius function fits and the MN equation, to the resistivity data of $Ge_{15}Te_{85}$ and $Ge_3Sb_6Te_5$ was conducted in a self-developed Matlab program using a least-square method.

Also, the TNM-AG model calculations and fitting to the fictive temperature data obtained from enthalpy and resistivity measurements are conducted according to the information given in the Supporting Information.

Supporting Information

Supporting Information is available from the Wiley Online Library or from the author.

Acknowledgements

The authors acknowledge funding in part from the Deutsche Forschungsgemeinschaft (DFG) via the collaborative research center Nanoswitches (SFB 917) and in part from the Federal Ministry of Education and Research (BMBF, Germany) in the project NEUROTEC II (16ME0398K). P.L. acknowledges funding from NSF-DMR grant No. 1832817. S.W. acknowledges the support of the DFG grant No. AOBJ670132. Support with the hardware and software of the electrical setup by Christoph Persch is greatly appreciated.

Open access funding enabled and organized by Projekt DEAL.

Conflict of Interest

The authors declare no conflict of interest.

Data Availability Statement

The data that support the findings of this study are available from the corresponding author upon reasonable request.

Keywords

data storages, glass dynamics, phase change materials, rejuvenation, resistance drifts, structural relaxations

Received: June 24, 2022
Revised: August 31, 2022
Published online: September 25, 2022

[1] S. R. Ovshinsky, *Phys. Rev. Lett.* **1968**, *21*, 1450.
[2] M. H. R. Lankhorst, B. W. Ketelaars, R. A. Wolters, *Nat. Mater.* **2005**, *4*, 347.
[3] S. Raoux, *Annu. Rev. Mater. Res.* **2009**, *39*, 25.
[4] D. Loke, T. H. Lee, W. J. Wang, L. P. Shi, R. Zhao, Y. C. Yeo, T. C. Chong, S. R. Elliott, *Science* **2012**, *336*, 1566.
[5] S. R. Elliott, *Inter. J. of Appl. Glass Sci.* **2015**, *6*, 15.
[6] K. Shportko, S. Kremers, M. Woda, D. Lencer, J. Robertson, M. Wuttig, *Nat. Mater.* **2008**, *7*, 653.
[7] M. Zhu, O. Cojocaru-Mirédin, A. M. Mio, J. Keutgen, M. Küpers, Y. Yu, J.-Y. Cho, R. Dronskowski, M. Wuttig, *Adv. Mater.* **2018**, *30*, 1706735.
[8] M. Wuttig, V. L. Deringer, X. Gonze, C. Bichara, J.-Y. Raty, *Adv. Mater.* **2018**, *30*, 1803777.
[9] J.-Y. Raty, M. Schumacher, P. Golub, V. L. Deringer, C. Gatti, M. Wuttig, *Adv. Mater.* **2019**, *31*, 1806280.
[10] Y. Cheng, O. Cojocaru-Mirédin, J. Keutgen, Y. Yu, M. Küpers, M. Schumacher, P. Golub, J.-Y. Raty, R. Dronskowski, M. Wuttig, *Adv. Mater.* **2019**, *31*, 1904316.
[11] S. Maier, S. Steinberg, Y. Cheng, C.-F. Schön, M. Schumacher, R. Mazzarello, P. Golub, R. Nelson, O. Cojocaru-Mirédin, J.-Y. Raty, M. Wuttig, *Adv. Mater.* **2020**, 2005533.
[12] B. J. Kooi, M. Wuttig, *Adv. Mater.* **2020**, *32*, 1908302.
[13] L. Guarneri, S. Jakobs, A. von Hoegen, S. Maier, M. Xu, M. Zhu, S. Wahl, C. Teichrib, Y. Zhou, O. Cojocaru-Mirédin, M. Raghuwanshi, C.-F. Schön, M. Drögeler, C. Stampfer, R. P. S. M. Lobo, A. Piarristeguy, A. Pradel, J.-Y. Raty, M. Wuttig, *Adv. Mater.* **2021**, *33*, 2102356.
[14] C. Persch, M. J. Müller, A. Yadav, J. Pries, N. Honné, P. Kerres, S. Wei, H. Tanaka, P. Fantini, E. Varesi, F. Pellizzer, M. Wuttig, *Nat. Commun.* **2021**, *12*, 4978.
[15] N. Yamada, E. Ohno, K. Nishiuchi, N. Akahira, M. Takao, *J. Appl. Phys.* **1991**, *69*, 2849.
[16] M. Wuttig, N. Yamada, *Nat. Mater.* **2007**, *6*, 824.
[17] D. Lencer, M. Salinga, B. Grabowski, T. Hickel, J. Neugebauer, M. Wuttig, *Nat. Mater.* **2008**, *7*, 972.
[18] A. Sebastian, M. L. Gallo, G. W. Burr, S. Kim, M. BrightSky, E. Eleftheriou, *J. Appl. Phys.* **2018**, *124*, 111101.
[19] A. Sebastian, M. L.e Gallo, R. Khaddam-Aljameh, E. Eleftheriou, *Nat. Nanotechnol.* **2020**, *15*, 529.
[20] D. Kuzum, R. G. Jeyasingh, B. Lee, H. S. Wong, *Nano Lett.* **2012**, *12*, 2179.
[21] T. Tuma, A. Pantazi, M. L.e Gallo, A. Sebastian, E. Eleftheriou, *Nat. Nanotechnol.* **2016**, *11*, 693.
[22] W. Zhang, E. Ma, *Mater. Today* **2020**, *41*, 156.
[23] K. Ding, J. Wang, Y. Zhou, H. Tian, L. Lu, R. Mazzarello, C. Jia, W. Zhang, F. Rao, E. Ma, *Science* **2019**, *366*, 210.
[24] W. W. Koelmans, A. Sebastian, V. P. Jonnalagadda, D. Krebs, L. Dellmann, E. Eleftheriou, *Nat. Commun.* **2015**, *6*, 8181.
[25] D. Ielmini, S. Lavizzari, D. Sharma, A. L. Lacaita, *Appl. Phys. Lett.* **2008**, *92*, 193511.
[26] S. Kim, B. Lee, M. Asheghi, F. Hurkx, J. P. Reifenberg, K. E. Goodson, H.-S. P. Wong, *IEEE Trans. Electron Devices* **2011**, *58*, 584.
[27] D. Krebs, R. M. Schmidt, J. Klomfaß, J. Luckas, G. Bruns, C. Schlockermann, M. Salinga, R. Carius, M. Wuttig, *J. Non-Cryst. Solids* **2012**, *358*, 2412.
[28] M. Wimmer, M. Kaes, C. Dellen, M. Salinga, *Fron. in Phy.* **2014**, *2*, 75.
[29] B. Kersting, S. G. Sarwat, M. Le Gallo, K. Brew, S. Walfort, N. Saulnier, M. Salinga, A. Sebastian, *Adv. Funct. Mater.* **2021**, 2104422.
[30] D. Ielmini, S. Lavizzari, D. Sharma, A. L. Lacaita, *IEEE Intern. Elec. Devices Meeting* **2007**, *1*, 939.
[31] M. Boniardi, D. Ielmini, *Appl. Phys. Lett.* **2011**, *98*, 243506.

[32] J.-Y. Raty, W. Zhang, J. Luckas, C. Chen, R. Mazzarello, C. Bichara, M. Wuttig, *Nat. Commun.* **2015**, *6*, 7467.
[33] M. L. Gallo, D. Krebs, F. Zipoli, M. Salinga, A. Sebastian, *Adv. Electron. Mater.* **2018**, *4*, 1700627.
[34] G. W. Scherer, *J. Non-Cryst. Solids* **1990**, *123*, 75.
[35] I. M. Hodge, *Science* **1995**, *267*, 1945.
[36] G. W. Scherer, *Relaxation in Glass and Composites*, John Wiley & Sons, Inc, New York **1986**.
[37] C. T. Moynihan, A. J. Easteal, M. A. Bolt, J. Tucker, *J. Am. Ceram. Soc.* **1976**, *267*, 1945.
[38] I. M. Hodge, A. R. Berens, *Macromolecules* **1981**, *14*, 1598.
[39] I. M. Hodge, A. R. Berens, *Macromolecules* **1982**, *15*, 762.
[40] H. N. Ritland, *J. Am. Ceram. Soc.* **1954**, *37*, 370.
[41] G. W. Scherer, *J. Am. Ceram. Soc.* **1986**, *69*, 374.
[42] J. Pries, S. Wei, F. Hoff, P. Lucas, M. Wuttig, *Scr. Mater.* **2020**, *178*, 223.
[43] J. Pries, Y. Yu, P. Kerres, M. Häser, S. Steinberg, F. Gladisch, S. Wei, P. Lucas, M. Wuttig, *Phys. Status Solidi RRL* **2021**, *15*, 2000478.
[44] Y. Yue, *J. Non-Crystalline Solids: X* **2022**, *14*, 100099.
[45] A. Q. Tool, *J. Am. Ceram. Soc.* **1946**, *29*, 240.
[46] O. S. Narayanaswamy, *J. Am. Ceram. Soc.* **1971**, *54*, 491.
[47] C. T. Moynihan, A. J. Easteal, J. Wilder, J. Tucker, *J. Phys. Chem.* **1974**, *78*, 2673.
[48] I. M. Hodge, *Macromolecules* **1986**, *19*, 936.
[49] G. Adam, J. H. Gibbs, *J. Chem. Phys.* **1965**, *43*, 139.
[50] C. T. Moynihan, in *Structure, Dynamics, and Properties of Silicate Melts* (Eds: J. F. Stebbins, P. F. McMillan, D. B. Dingwell), Walter de Gruyter, Berlin, Germany **1995**, pp. 1–20.
[51] L. J. van der Pauw, *Philips Res. Rep.* **1958**, *13*, 1.
[52] J. Pries, H. Weber, J. Benke-Jacob, I. Kaban, S. Wei, M. Wuttig, P. Lucas, *Adv. Func. Mater.* **2022**, *32*, 2202714.
[53] S. Wei, P. Lucas, C. A. Angell, *MRS Bull.* **2019**, *44*, 691.
[54] H. N. Ritland, *J. Am. Ceram. Soc.* **1956**, *39*, 403.
[55] S. Spinner, A. Napolitano, *J. Res. Nat. Bur. Stand. – A. Phy. and Chem.* **1966**, *70A*, 147.
[56] M. M. Hurley, P. Harrowell, *Phys. Rev. E* **1995**, *52*, 1694.
[57] M. D. Ediger, *Annu. Rev. Phys. Chem.* **2000**, *51*, 99.
[58] L. Berthier, *Phy.* **2011**, *4*, 42.
[59] M. D. Ediger, P. Harrowell, *J. Chem. Phys.* **2012**, *137*, 080901.
[60] P. B. Macedo, A. Napolitano, *J. Res. Nat. Bur. Stand. – A. Phy. Chem.* **1967**, *71A*, 231.
[61] J. Pries, S. Wei, M. Wuttig, P. Lucas, *Adv. Mater.* **2019**, *31*, 1900784.
[62] J. Pries, J. C. Sehringer, S. Wei, P. Lucas, M. Wuttig, *Mater. Sci. Semicond. Process.* **2021**, *134*, 105990.
[63] L. Calvez, Z. Yang, P. Lucas, *Optics Express* **2009**, *17*, 18581.